

Radiologic imaging of the renal parenchyma structure and function

Nicolas Grenier¹, Pierre Merville² and Christian Combe³

Abstract | Radiologic imaging has the potential to identify several functional and/or structural biomarkers of acute and chronic kidney diseases that are useful diagnostics to guide patient management. A renal ultrasound examination can provide information regarding the gross anatomy and macrostructure of the renal parenchyma, and ultrasound imaging modalities based on Doppler or elastography techniques can provide haemodynamic and structural information, respectively. CT is also able to combine morphological and functional information, but the use of CT is limited due to the required exposure to X-ray irradiation and a risk of contrast-induced nephropathy following intravenous injection of a radio-contrast agent. MRI can be used to identify a wide range of anatomical and physiological parameters at the tissue and even cellular level, such as tissue perfusion, oxygenation, water diffusion, cellular phagocytic activity, tissue stiffness, and level of renal filtration. The ability of MRI to provide valuable information for most of these parameters within a renal context is still in development and requires more clinical experience, harmonization of technical procedures, and an evaluation of reliability and validity on a large scale.

Chronic kidney disease (CKD) and acute kidney injury (AKI) are characterized by distinct changes in renal morphology and function that are typically assessed using measures of proteinuria or estimated glomerular filtration rate (eGFR), but these changes could be better defined through the use of radiologic techniques at disease initiation and during follow-up. The development and validation of new biomarkers that can characterize changes in renal tissue composition or help predict clinical and functional outcomes in native and transplanted kidneys is of great interest to practicing nephrologists. Noninvasive radiologic imaging techniques can be used in concert with biological (chemical or molecular) biomarkers to identify the activation of renal pathophysiological pathways^{1,2}, with the possibility of noninvasive monitoring over time using serial assessments. Among the most commonly practiced imaging techniques, MRI has the highest range of applications, with the ability to provide information on parameters such as changes in tissue perfusion and oxygenation, water diffusion, cellular phagocytic activity, tissue stiffness, and the functional level of renal filtration. CT and grey-scale and Doppler ultrasonography can also provide information on some of these functional and structural parameters; however, despite extremely encouraging preclinical and preliminary clinical results, the reliability of these

methods in further defining renal injury is yet to be proven. More clinical experience and a harmonization of technical requirements is required before these radiologic methods can be considered and validated against current diagnostic methods.

Many of the techniques discussed in this Review require intravenous administration of a contrast agent to enhance visibility and imaging, particularly of blood vessels, but this approach carries the risk of contrast-induced nephropathy or nephrogenic systemic fibrosis. Reviews on this topic can be found elsewhere^{3,4}. This Review emphasizes the potential of the radiologic imaging techniques that can help analyse the main functional and structural processes involved in renal parenchymal diseases, namely changes in macrostructure (kidney volume, corticomedullary differentiation (CMD), and cystic disease), microstructure (development of intrarenal inflammation and fibrosis), and functional changes in renal blood flow, perfusion, and oxygenation, and renal filtration. Nuclear imaging techniques and morphological imaging of pre-renal vessels and the post-renal excretory system are not included in this Review. We assess the strengths and weaknesses of each imaging technique, the level of validation that has been reached thus far, and the ability of radiologic imaging to provide useful information to help direct patient management.

¹Service d'Imagerie Diagnostique et Interventionnelle de l'Adulte, Centre Hospitalier Universitaire de Bordeaux, Groupe Hospitalier Pellegrin, Place Amélie Raba-Léon, 33076 Bordeaux Cedex, France.

²University of Bordeaux, Rue Léo Saignat, 33076 Bordeaux Cedex, France.

³Service de Néphrologie Transplantation Dialyse, Centre Hospitalier Universitaire de Bordeaux, Groupe Hospitalier Pellegrin, Place Amélie Raba-Léon, 33076 Bordeaux Cedex, France.

Correspondence to N.G. nicolas.grenier@chu-bordeaux.fr

doi:10.1038/nrneph.2016.44
Published online 12 Apr 2016

Key points

- Radiologic techniques can be used to assess gross renal morphology, but morphological changes at this level show poor correlation with renal function and the changes over time are often nonspecific
- Dynamic contrast-enhanced CT or MRI can provide haemodynamic information, such as renal blood flow or tissue perfusion, which can facilitate personalized patient management
- Information obtained from blood oxygen level-dependent MRI could contribute to the understanding of chronic kidney disease pathophysiology, but technical issues remain to be solved before large-scale clinical use
- MRI and renal scintigraphy can both provide a measure of split renal function in moderately dilated kidneys, but radiological measurement of single kidney glomerular filtration rate requires further development
- The ability to identify fibrotic changes and inflammatory components in damaged renal tissue by radiologic imaging is a major goal for future research

MRI

Imaging modality that uses a strong oscillating magnetic field to induce endogenous atoms to emit radiowaves that are detected and used to generate 2D and 3D images of a living subject.

CT

An imaging modality that processes and combines X-ray images to produce tomographic (slice) images. CT provides cross sectional images of organs, bones, soft tissues in multiple planes.

Doppler ultrasonography

Doppler ultrasound estimates blood flow through vessels by bouncing high-frequency sound waves off circulating red blood cells.

Corticomedullary differentiation

(CMD). Visualizes the differences in intensity, echogenicity, or attenuation between cortical and medullary compartments of the kidney, and can be a biomarker of renal insufficiency.

Ultrasonography

Visualization of deep body structures based on a recording of the reflections or echoes of ultrasonic pulses directed into the tissue. Frequencies of the pulses typically range from 1.6 MHz to 10 MHz.

Tesla (T)

Unit of measurement to quantify the strength of a magnetic field. Clinical MRI scanners operate at a level of 1.5T or 3T.

Technical advances in clinical imaging

Continuous technical developments over the past 10 years have led to an improvement in the performance of most radiologic techniques. Ultrasonography has developed into a multi-parametric imaging tool that can provide morphological information at a high resolution due to the development of high-frequency probes (FIG. 1), information on haemodynamics due to the incorporation of Doppler, information on tissue perfusion when used with new contrast agents, and structural information when combined with elastographic techniques. The increase in the density of detectors on CT detector rows has led to improvements in the spatial and temporal resolution of functional acquisitions, and the resolution is now isotropic (equal in all three dimensions). New algorithms that use dual-energy CT for image reconstruction have enabled the dose of radiation to be markedly reduced and for a spectral display of density values, which might enable even more specific tissue characterization in the future. Finally, new, high-field clinical MRI systems that operate at a magnetic field strength of 3 tesla (T) instead of 1.5T, have improved the signal-to-noise ratio and consequently the spatial resolution of the images. Unfortunately, increased spatial resolution raises the level of sensitivity to artefacts that are often produced when imaging the abdomen. As a result, the utility of 3T MRI devices for imaging the renal parenchyma remains subject of debate.

Changes in renal macrostructure

Renal volume

Numerous studies have identified a potential association between the functional parenchymal volume and glomerular filtration and/or renal functional reserve^{5,6}. Measurement of the kidney long axes (renal length) by ultrasonography is currently the only method employed to estimate functional renal volume, for practical reasons. Several studies that have aimed to identify a correlation between long-axis values and parenchymal volume have produced contradictory results⁵⁻⁷, suggesting that the use of this measurement as a biomarker of functional parenchymal volume could be inaccurate. An abnormally small kidney will inherently exhibit diminished functional capacity that cannot be recovered, but in some

cases, the kidneys might exhibit chronic and/or irreversible dysfunction with a delayed volume reduction, as observed in patients with diabetic nephropathy⁸.

An accurate assessment of the functional parenchymal volume would be of value in clinical practice, and the use of imaging to calculate actual parenchymal volumes from 3D CT or MRI acquisitions and automatic or semi-automatic 3D post-processing techniques would be worthwhile (see [Supplementary information S1](#) (figure)). Several studies that have used customized imaging software have demonstrated a high correlation between measurements of renal and cortical volumes and the reference methods in both animal ($r=0.86-0.99$)^{6,7} and human kidneys (1.25 ml maximal standard deviations of the differences)^{6,7,9}. Measurements of renal volume by MRI correlate better with single kidney glomerular filtration rate (GFR) ($r=0.86$) than does renal bipolar length ($r=0.78$)¹⁰. Unfortunately, these methods are still not widely available to most clinicians.

Corticomedullary differentiation

Determining the degree of separation between the renal cortex and the medulla by imaging analysis is important, as these two compartments perform different physiological functions and are affected by different pathophysiological mechanisms during renal disease. Normal CMD is readily visible by ultrasound or T1-weighted and T2-weighted MRI, but as the renal cortex and the medulla have the same density (~30 Hounsfield units), assessment of CMD by CT requires injection of a contrast agent.

CMD tends to decrease or disappear in patients with AKI or CKD (in both native and transplanted kidneys), with no clear correlation to the level of serum creatinine¹¹. Interestingly, CMD has been shown by MRI to reappear upon restoration of renal function¹². The correlation between tissue changes and signal intensity changes detected by MRI (or level of echogenicity in ultrasound) are not fully understood and are subject to speculation¹³. Conversely, reversed CMD can be observed by ultrasonography in several specific diseases (including nephrocalcinosis, Tamm–Horsfall proteinuria, recessive polycystic disease, and haemoglobinuria)¹³. A strong decrease in cortical signal intensity that is visible by T2-weighted MRI can be observed in patients with cortical necrosis or those with hemosiderin deposition due to haemolysis in conditions such as paroxysmal nocturnal haemoglobinuria or sickle cell disease¹⁴.

Cystic diseases of the kidney

Various techniques have been used to evaluate disease state and progression in patients with autosomal dominant polycystic kidney disease (ADPKD)¹⁵. MRI is now the preferred method over ultrasonography to measure renal cysts and kidney volume for the follow-up of patients with ADPKD, due to improved reliability of the data¹⁶. A landmark study documented an inverse correlation between total cyst and kidney volumes and renal function, with a parallel and well-correlated evolution of these parameters over time¹⁷. The annual rate

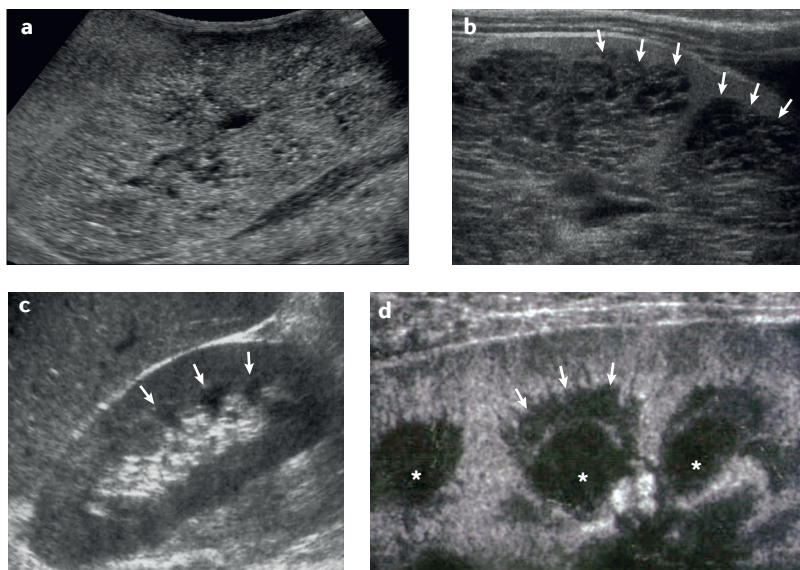


Figure 1 | Sonographic changes in autosomal recessive polycystic kidney disease. **a** | Ultrasonography using a low-frequency probe detects hyperechoic regions in an enlarged kidney; corticomedullary differentiation is lost. **b** | A high frequency probe is required to identify the corticomedullary junction and numerous tiny medullary cysts spreading from the corticomedullary junction (arrows) to the renal papilla. **c** | Ultrasonography using a low frequency probe of a normal adult right kidney with a hypoechoic inner medulla (arrows). **d** | Ultrasonography using a high frequency probe of a normally functioning transplanted kidney with clear identification of the corticomedullary junction that separates the cortex and outer medulla (arrows) and hypoechoic inner medulla (asterisks).

of percentage change in total kidney volume evaluated by MRI was selected as the primary objective in another study that demonstrated the efficiency of tolvaptan in patients with ADPKD¹⁸. The utility of this biomarker has since been challenged, as eGFR is now considered a more clinically useful variable. Clinical evaluation and genetic testing for cystic kidney diseases has been described elsewhere¹⁹.

Changes in renal microstructure

The most notable changes to renal microstructure that guide patient management and diagnosis include inflammation (that occurs during the acute phases of kidney diseases) and the progressive deposition of collagen, causing glomerular and interstitial fibrosis. Several techniques based on ultrasonography and MRI have been proposed as a means to detect and quantify these events, but these procedures cannot differentiate between fibrosis and inflammation, which can both modify the results in the same way.

Intrarenal inflammation

The extent of renal inflammation in the kidney in patients with diffuse renal parenchymal disease can only be assessed by renal biopsy, which remains the gold standard. However, an assessment of the evolution of renal inflammation, such as the density of inflammatory cells (macrophages, leukocytes, and lymphocytes) in the renal parenchyma, might also be clinically useful. For example, patients with lupus nephritis often require several renal biopsies throughout the course of their

disease to assess inflammation. Radiologic techniques could instead provide an estimate of the intensity of renal inflammation, as opposed to monitoring renal fibrosis, and could be helpful when making therapeutic decisions and/or in monitoring a response to treatment. A similar approach could potentially be useful for patients who have received a kidney transplant, in whom renal biopsies are repeatedly performed to assess several parameters, including the degree of renal inflammation. A radiologic approach would only be valuable, however, if measures of inflammation to diagnose allograft rejection (according to the Banff classification system) are demonstrated to correlate with the degree of signal intensity changes.

Strategies to visualize inflammatory cells or target different types of molecules involved in the inflammatory process (for example integrins or complement fractions) have been developed based on an MRI approach that incorporates the administration of superparamagnetic iron oxide (SPIO) particles. Evaluation of inflammatory cells requires an injection of ultra-small SPIO (USPIO) contrast particles that are ~20 nm in diameter and have a long half-life in the blood stream (2 h in rats and 36 h in humans). Larger SPIO particles of 120–180 nm have a short half-life of ~2 h in humans and are avidly captured by extra-hepatic cells with phagocytic activity, including blood circulating monocytes and tissue resident macrophages, as well as by the liver and spleen²⁰. USPIOs produce a magnetic susceptibility effect (as observed with deoxyhaemoglobin) that is identified by a decrease in signal intensity on T2*-weighted sequences. USPIO accumulation within a tissue induces a strong decrease in signal intensity on gradient-echo T2*-weighted sequences, which exhibit a higher sensitivity compared to regular spin-echo T2-weighted sequences.

Several rat models of experimental nephropathy, including nephrotic syndrome²⁰, hydronephrosis²¹, anti-glomerular basement membrane glomerulonephritis²¹, acute graft rejection²², acute tubular necrosis induced by ischaemia-reperfusion²³, and chronic graft rejection²⁴, have been used to demonstrate the detectability of intrarenal macrophagic activity by USPIO-mediated MRI. In all of these models, a decrease in intrarenal signal intensity was observed 24 h after injection of USPIOs and correlated with the number of macrophages within each renal compartment ($r=0.88$) and with the severity of disease ($r=0.89$). The decreases in signal intensity involved both the cortex and the medulla in all but two of the models of nephropathy (the anti-glomerular basement membrane model, where the drop of signal intensity involved the cortex, exclusively²¹, and the ischaemia-reperfusion model that only involved the medulla²³).

A small, clinical pilot study performed in 12 patients with either native or transplanted kidneys confirmed the findings from the rat nephropathy models described above²⁵. All patients with an inflammatory component of renal disease identified on cortical biopsy, including acute graft rejection, showed a marked decrease in diffuse signal intensity within the renal parenchyma (i.e. involving the cortex and medulla) after USPIO particle

Superparamagnetic iron oxide particles (SPIO) Iron oxide (magnetite and maghemite) particles 150 nm in size that exhibit superparamagnetism and can be used to label cells and monitor them in real time.

injection, whereas patients with chronic and fibrotic disease without inflammatory components on biopsy did not exhibit this change in signal intensity. More interestingly, and consistent with preclinical studies, three patients with acute tubular necrosis (two with transplanted kidneys and one with native kidneys) exhibited a marked decrease in signal intensity within the medulla only — a zone that is usually not accessible for percutaneous renal biopsy (FIG. 2). Although Sinerem® (Guerbet, France) did not gain authorization for clinical use, another USPIO-agent, Feraheme® (AMAG Pharmaceuticals, USA), was approved in North America and Europe for the treatment of anaemia in CKD. This agent has been evaluated in normal kidneys²⁶, but the severe allergic reactions it can induce precludes its use in routine imaging.

Complex, experimental imaging approaches to identify inflammatory processes in the kidney have been proposed, such as monitoring the homing of SPIO-labelled macrophages readministered intravenously²⁷, or using SPIOs conjugated to recombinant complement receptor type 2 that will specifically bind to renal C3 deposits^{28,29}. A similar approach based on microbubbles conjugated with anti-human CD3 antibody to target human lymphocytes that are then followed using ultrasonography, has also been proposed³⁰. These elegant strategies are currently restricted by regulatory policies, but they could lead to interesting developments in the future.

Intrarenal fibrosis

Quantification of fibrosis and evaluation of its evolution over time could be a useful measurable parameter in most cases of CKD; such data obtained by radiologic imaging would be complementary to the biological markers used to evaluate GFR. The methods by which intrarenal fibrosis can be quantified are outlined below.

Quantification of renal echogenicity. Studies have shown that compared to renal size, cortical thickness, or parenchymal thickness, renal echogenicity has the strongest correlation with renal histological parameters, such as glomerular sclerosis, tubular atrophy, interstitial fibrosis, and interstitial inflammation ($r=0.28-0.35$)³¹. This correlation coefficient, however, is still very low, and thus the predictive value of renal echogenicity is relatively poor. Unfortunately, no distinction between inflammation and fibrosis can be demonstrated by visualizing renal echogenicity. A close association between echogenicity and renal function in patients with a right solitary kidney has been shown, but no insight into the underlying pathological processes has been provided³². Alternative methods need to be developed and validated for this purpose.

Magnetic resonance diffusion-weighted imaging.

Diffusion-weighted magnetic resonance sequences are T2-weighted sequences that encode microscopic movements of protons in three orthogonal directions when specific gradient characteristics (b-values) are used. These sequences can provide data regarding microscopic movements and exchange of water molecules between intracellular and extracellular spaces. A map of the apparent diffusion coefficient (ADC) can be generated when several b-values are used in the sequence followed by application of a specific, post-processing algorithm.

Several studies have shown that ADC values are higher in the cortex than in the medulla of healthy kidneys^{33,34}. Unfortunately, comparison of absolute ADC values (obtained at different centres or from different studies) is difficult because they are influenced by the type of b-value used². The ADC decreases with increasing renal dysfunction, probably owing to a decrease in water exchange and an increase in biological barriers within the tissues, such as regions of fibrosis³⁵. Most studies have focused on comparing ADC values with eGFR, and only one preclinical study has reported a correlation between ADC values and the degree of intrarenal collagen deposition ($R^2=0.57$) in a model of unilateral hydronephrosis³⁶. To our knowledge, no clinical study has compared the association between ADC values and collagen deposition.

Diffusion tensor imaging (DTI) is a variation to diffusion-weighted MRI, and applies six or more directions to encode proton movement to facilitate the detection of specific directions of movement of protons that predominate within the tissue. This method generates a value of fractional anisotropy — the percentage of a tissue that displays oriented diffusion axes (FIG. 3). The liver is a fully isotropic structure, with a random microstructural orientation, whereas the kidney is characterized by its anisotropic architecture. The predominant orientations of renal microstructures lie in the direction of the axis of

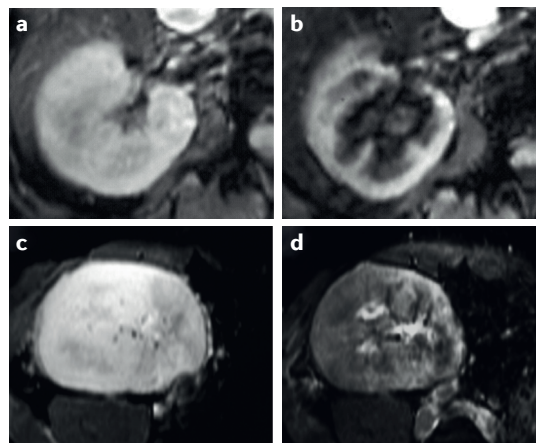


Figure 2 | Visualization of intrarenal post-inflammatory phagocytic activity with ultrasmall supermagnetic iron oxide (USPIO)-enhanced T2*-weighted magnetic resonance sequences. a | Renal magnetic resonance image of a patient with acute tubular necrosis before injection with USPIO particles. The renal parenchyma is homogeneously hyperintense. **b** | A low signal intensity, due to phagocytosis of the USPIO particles, is observed in all renal pyramids 3 days after injection of the particles. **c** | Renal magnetic resonance image of a patient with acute rejection of a renal allograft before injection of USPIO particles. The renal parenchyma is homogeneously hyperintense. **d** | A marked drop in signal intensity is observed in all renal compartments 3 days after injection of USPIO particles. This effect is due to phagocytosis of iron oxide particles by macrophages.

Apparent diffusion coefficient (ADC)

A measure of the magnitude of diffusion of water molecules within a tissue that is calculated using MRI with diffusion weighted imaging. The ADC provides an assessment of tissue integrity.

Diffusion tensor imaging (DTI)

A technique to measure the restricted diffusion of water according to the major direction of tissue architecture. DTI enables characterization of microstructural changes by measuring the fractional anisotropy and orientation of the diffusion tensor

Fractional anisotropy

Indicates the percentage of a tissue that displays oriented diffusion axes and is a reflection of tissue microstructure.

each medulla (cortex-to-papilla), which helps guide the movement of water along the medullary rays. In healthy kidneys, the percentage of orientation within the medulla is higher than in the cortex (39% versus 22%), due to the presence of medullary rays³⁷.

The ADC (obtained by diffusion technique) and degree of fractional anisotropy (obtained by DTI) are thought to be complementary measures, as the ADC provides information on the total diffusion value within the tissue (the level of water exchange), and fractional anisotropy reflects the tissue microstructure. These two data points could be used as an architectural biomarker of fibrosis in CKD, as the fibrotic process leads to progressive destruction of the renal microarchitecture.

Elastography. The evaluation of chronic liver diseases has been improved by combining ultrasound elastography (applying stress and detecting tissue displacement by ultrasound) with biological criteria to evaluate the degree of fibrosis. Integration of elastographic information to the management of CKD might also be of benefit. Several single-centre studies have reported mixed results from initial experiences with elastography in the analysis of transplanted kidneys. Discrepancies in the data are caused by several factors. First, several techniques are available to perform ultrasound elastography, each with different principles, advantages, and drawbacks³⁸. Quasi-static elastography (also known as real-time elastography) is based on a quasi-static deformation or strain of the medium that is often achieved by compressing the tissue with a probe. This approach is simple to implement but provides only qualitative information or semi-quantitative surrogate parameters of tissue stiffness³⁹, such as the elasticity ratio⁴⁰ or fibrosis index⁴¹. Alternative techniques have been developed based on the measurement of the shear wave velocity (SWV) in order to circumvent the lack of quantitative data, as discussed below.

Three main quantitative methods based on SWV are available: transient elastography (using the FibroScan®; Echosens, France), acoustic radiation force impulse (ARFI; Siemens Medical Solutions, USA) and supersonic shear imaging (SSI; using the Aixplorer®; Supersonic Imagine, France) (FIG. 4). In our opinion, the FibroScan® transient elastography system (currently used to assess liver fibrosis) is inappropriate for renal sampling as all of the measurements are made in one dimension. Furthermore, there is no control over the position of the sample volume by real time sonography and the sample volume is fixed in depth and size. Moreover, the mechanical wave has to be applied from the surface of the skin, which can interfere with the measurements as the shear wave must travel through numerous layers of tissue before it reaches the target organ.

Quantitative ARFI is also a one-dimensional method, and measures SWV in m/s in a sample volume of 5 mm³. In contrast with transient elastography, the shear waves are generated directly within the organ. Finally, SSI based on a combination of ARFI and ultrafast ultrasound imaging provides a 2D map of elasticity (in m/s or kPa). ARFI and SSI seem to be the most appropriate methods

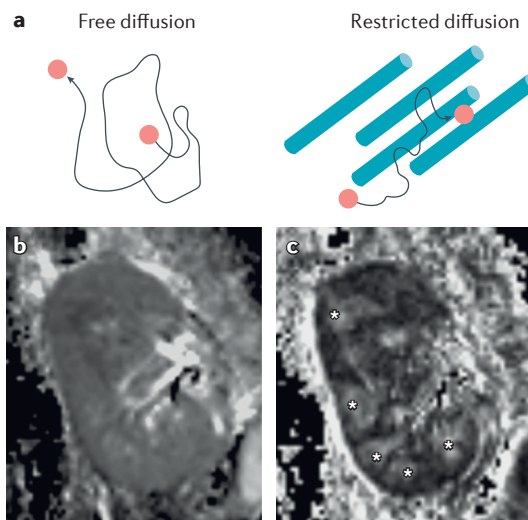


Figure 3 | Diffusion-weighted MRI and diffusion tensor imaging in a kidney transplant. **a** | Diffusion-weighted magnetic resonance sequences encode microscopic water movements. These movements can either be randomly oriented and display a free diffusion pattern (isotropic), or exhibit a predominant orientation related to tissue microstructures and are thus restricted in their diffusion pattern (anisotropic). **b** | A coronal map of the apparent diffusion coefficient (ADC) of a normal renal transplant that is produced by encoding the microscopic water movements in three directions. No clear difference in the ADC values is evident between the cortex and medulla. **c** | When encoding microscopic water movements in at least six directions, a map of the fractional anisotropy can be produced (the percentage of selectively oriented water movements). On this coronal map of the fractional anisotropy, all pyramids are brighter than the surrounding (asterisks), indicating the presence of a higher fractional anisotropy value within medulla compared to the cortex. This higher anisotropy is caused by the high density of medullary rays with tubules and vessels oriented toward papillae.

for renal imaging, but all three systems described are sensitive to the anisotropy (microstructure) of the renal parenchyma, external or internal pressure due to compression by the probe (mainly on superficial transplants), and perfusion or urinary pressure^{42–44}. These factors render the application of ultrasound elastography for renal imaging more problematic than for the liver, and must be considered before extending this method to large clinical trials.

Two studies that used quantitative methods to evaluate fibrosis have reported that SWV (by ARFI) in native kidneys correlates with eGFR and the stage of CKD^{45,46}. In both studies, however, the SWV decreased (indicating softer tissue) with a decrease in GFR. These findings are in contrast to those from patients with liver disease; this surprising discrepancy is yet to be explained. A third study that used the same methodology could not predict the different stages of CKD and no correlation was found with any pathological indicators of fibrosis. Contradictory results have also been reported in the context of diabetic nephropathy^{47,48}.

Shear wave velocity (SWV)

Shear waves are an elastic waveform that move as a shear or transverse wave through the body of an object. The SWV is a measure of tissue stiffness in m/s.

Transient elastography

An ultrasound-based form of transient elastography developed by FibroScan that measures the extent of fibrosis and quantifies steatosis.

Acoustic radiation force impulse (ARFI)

A form of ultrasound elastography that uses acoustic radiation forces (< 1 ms) to assess tissue stiffness and stage fibrosis.

Supersonic shear imaging (SSI)

An ultrasound-based technique for real time visualization of soft tissue viscoelastic properties. SSI provides a measure of tissue stiffness.

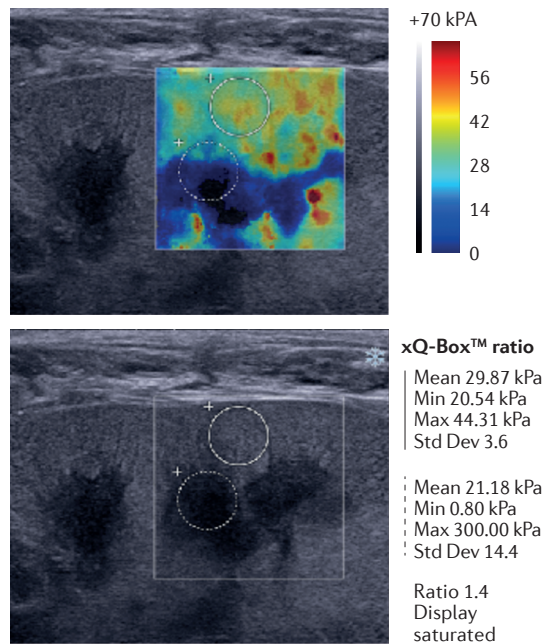


Figure 4 | Ultrasound-elastography using shear wave imaging technique on a renal allograft. The top panel shows a quantitative 2D colour map of elasticity on the anterior aspect of the kidney using a high-frequency probe. The colour map illustrates higher tissue stiffness in the cortex compared to the medulla. The bottom panel shows two regions of interest: the cortex (upper region of interest) and medulla (lower region of interest), where measurements of elasticity (kPa) can be made. In this example, the cortical elasticity is 29.87 kPa and medullary elasticity value is 21.18 kPa.

By using the SSI technique in transplanted kidneys, we found that renal cortical stiffness did not correlate with any clinical parameters, any single semi-quantitative item of allograft rejection according to the Banff score, or the level of interstitial fibrosis. A significant correlation ($r=0.41$, $P=0.03$) was obtained between cortical stiffness and the total Banff scores of all lesions, whereby all elementary lesions (vascular, interstitial, glomerular, and tubular lesions), chronic or not, were summed⁴⁹. These results suggest that elastography is probably more difficult to apply to renal analyses than to the liver, and an increase in tissue stiffness seems to reflect global, but not specific, tissue changes.

Emerging methods

Other methods based on magnetic resonance have been proposed to predict or assess the degree of tissue fibrosis, but only very preliminary results have been generated in the context of the kidney. Magnetic resonance elastography is a technique that can feasibly be applied to the kidney, but clinical experience is extremely limited⁵⁰. Further experience with this method is essential before it can be used for patient management.

Specific contrast agents that target collagen fibres have been tested within the heart^{51–53}, but no renal application has thus far been instigated. Quantification of the relaxation time (T1) of the tissue using a T1-mapping

method can reflect the concentration of macromolecules in the target tissue, such as collagen, and thus provides an indicator of tissue remodelling. T1-mapping was shown to be a good marker of chronic cardiac dysfunction⁵⁴ but experience within the kidney has been limited to experimental AKI⁵⁵. T1-mapping can be sensitized by measuring the magnetization transfer effect between free water protons and protons linked to macromolecules using specific magnetic resonance sequences⁵². The amount of transfer of magnetization is responsible for a signal decrease that is proportional to the concentration of these macromolecules⁵⁶. A good correlation has been found between the magnetization transfer ratio and eGFR in patients ($r=-0.645$)⁵⁷.

Renal fat fraction

Lipotoxicity has been linked to the pathogenesis of diabetic nephropathy and renders the glomeruli and renal tubules more susceptible to hypoxia. One study showed that specific magnetic resonance sequences, known as chemical shift-selectives, could measure renal lipid accumulation in a genetic mouse model of diabetes (db/db)⁵⁸. Application of these sequences and their clinical impact needs to be demonstrated.

Cell therapy imaging

Cellular regeneration techniques that use mesenchymal stem cells (MSCs)⁵⁹ or human renal progenitor cells⁶⁰ have been performed in the context of AKI in an attempt to accelerate the recovery of renal function and/or prevent the development of CKD. An imaging method to monitor the homing of injected stem cells was proposed that aimed to compare the efficiency of intra-arterial and intravenous cell grafting. After intra-arterial administration of SPIO-labelled MSCs, a strong decrease in signal intensity was observed *in vivo* within the cortex as late as 7 days after injection, and the iron-loaded MSCs were identified in renal glomeruli by histologic analysis^{61,62}. In a rat model of mesangiolytic, a homing effect of magnetically-labelled MSCs administered intravenously was detected *ex vivo* using very high field MRI (9.4 T) (see [Supplementary information S2](#) (figure)), but a large proportion of the cells were trapped within the liver, precluding their detection in the kidneys *in vivo* using lower field MRI (1.5 T)⁶³. On comparing the renal segments that showed a change in signal in *ex vivo* images with pathological lesions identified on histological sections, the areas of low signal intensity correlated well with α -actin expression (a marker of mesangial activation) and Prussian blue staining (a marker of iron-loaded MSCs). These data suggest that the MSCs specifically homed to injured tissues and this technique confirmed the selective homing of stem cells to diseased areas of the kidneys in this rat model.

Renal functional parameters

Renal circulation

The evaluation of intrarenal haemodynamic parameters could be complementary to imaging of the renal arteries. In various clinical situations, such as renovascular hypertension or hypertensive and/or diabetic nephropathy, an

Relaxation time (T2*)
Time constant for signal decay in MRI that uses a T2*-weighted gradient-echo sequence. T2* is the inverse of the rate of signal decay R2*.

accurate evaluation of blood flow, tissue perfusion, and oxygenation in various compartments of the kidney could be a useful indicator of disease status with potential predictive value, given the paramount importance of these parameters in mediating renal function.

Renal blood flow and tissue perfusion. Renal blood flow can be characterized and even measured without injection of any contrast agent, by using cine phase-contrast MRI. As with Doppler sonography, this method enables evaluation of the intra-arterial velocity profile and, by measuring the arterial diameter, quantification of renal blood flow in each renal vessel. Researchers have shown that a decrease in renal blood flow occurs before a reduction in GFR in patients with ADPKD, and is inversely associated with an increase in kidney volume. Furthermore, a decrease in renal blood flow is predictive of further progression of ADPKD, in terms of kidney volume and function⁶⁴. This measurement, however, has yet to be compared to reference methods and the level of variability is unknown. The utility of a velocity profile to provide haemodynamic information in renovascular disease has been shown to facilitate the quantification of renal artery stenosis⁶⁵.

A measurement of renal perfusion (volume of blood flow per gram of tissue and per unit of time) can be obtained by making dynamic contrast-enhanced (DCE) acquisitions with ultrasonography, CT or MRI or by using non-contrast magnetic resonance sequences, where the signal is generated only by the proton flow within the microvessels (known as arterial spin labelling). The latter approach seems very attractive in the context of renal insufficiency as it does not require injection of a gadolinium-based contrast agent; however, although this method seemed promising when measuring brain perfusion, its application in assessing the renal vasculature is technically challenging and is still under development⁶⁶.

DCE acquisitions facilitate progressive, visible enhancement of the renal parenchyma. When using CT or MRI, a renal perfusion value can be calculated based on signal intensity time curves, provided that the time resolution of the acquisitions is sufficiently high. Obtaining the renal perfusion value requires sampling of the signal intensity changes within the kidney and the aorta to characterize the arterial input function (the shape of the bolus of contrast) (see [Supplementary information S3](#) (figure)). Although this procedure is simple to implement, quantification of perfusion with DCE-ultrasonography remains difficult due to attenuation effects, destruction of microbubbles by the ultrasound beam, and absent arterial input function, despite several attempts using animal models. Perfusion-derived parameters can, however, be calculated using this method⁶⁷, and the technique is very efficient for detecting intrarenal perfusion defects (infarcts or cortical necrosis) in native and transplanted kidneys⁶⁸.

Quantitative values of perfusion in ml/min per gram of tissue can be obtained from DCE-CT and DCE-MRI by applying dedicated pharmacokinetic compartment models (FIG. 5). Quantification of renal perfusion in

pigs by DCE-CT showed strong correlation with a reference method that tracks injected fluorescent microspheres ($r=0.93$)⁶⁹. Low doses of gadolinium chelates (one-third or one-fourth of a clinical dose) are used in DCE-MRI. The relationship between signal intensity and gadolinium-chelate concentration is biphasic and nonlinear, and therefore, a conversion of the signal intensity into concentration is necessary, which is possible by several methods⁷⁰. CT has an advantage over MRI for this purpose as a linear relationship exists between density values and concentration of the iodine contrast agent. Although DCE-CT perfusion values have been validated in pigs (as described above)⁶⁹, MRI has been more widely studied most likely to circumvent the risks that are incurred with DCE-CT — namely excessive exposure to radiation and, to a lesser degree, iodine contrast nephropathy. DCE-MRI is able to detect global perfusion impairment but, to our knowledge, no validation with reference methods has yet been demonstrated. As a result, only severe haemodynamic changes and comparative data can be taken into account in pathological conditions (from kidney-to-kidney or territory-to-territory)⁷¹. More details on the principles, advantages, and limitations of these different models are available in the literature^{72,73}.

Renal tissue oxygenation. Maintaining a stable partial pressure of oxygen (pO_2) within the renal parenchyma depends on numerous adaptive mechanisms. Tissue oxygenation is of paramount importance in the context of AKI and CKD⁷⁴. The outer medulla is much more sensitive to hypoxia than is the cortex (pO_2 10–20 mmHg versus 50 mmHg), due to low blood flow and high oxygen consumption (~80%) as a consequence of active water and sodium reabsorption by Na^+K^+ -ATPase pumps along the thick ascending limb of the loop of Henle. This physiology renders the kidney highly susceptible to hypoxic injury, and it is now well established that chronic hypoxia is a major contributor to the development of parenchymal fibrosis and CKD, as observed in diabetic nephropathy^{75,76}. Changes in tissue oxygenation might be related to changes in either tissue perfusion, oxygen consumption, or both. Thus, any disease that induces an increase in tubular function (such as diabetes mellitus or unilateral nephrectomy), or decreases medullary perfusion (such as in contrast-induced nephropathy), could shift the balance toward hypoxia⁷⁷.

The only non-invasive *in vivo* technique that is able to assess regional oxygenation of the renal parenchyma is blood oxygen level-dependent (BOLD)-MRI. By using specific, dedicated sequences (multi-echo $T2^*$ -weighted sequences), a decrease in signal intensity can be observed within tissues with a low pO_2 that is associated with a decrease in relaxation time ($T2^*$). Quantitative maps of the relaxation time and of the relaxation rate ($R2^*$) can be generated, knowing that $R2^*$ is the inverse of $T2^*$ (see [Supplementary information S4](#) (figure)). The sensitivity of $T2^*$ -weighted sequences to oxygen levels is due to the paramagnetism that is exhibited by deoxyhaemoglobin but not oxyhaemoglobin. In accordance with the renal physiology, the medullary $T2^*$ -value is shorter than the

Dynamic contrast-enhanced (DCE)

Intravenous administration of a contrast agent prior to MRI or CT to facilitate quantification of physiological parameters in comparison to baseline (no contrast) images. Functional information such as perfusion, permeability, and renal filtration can be obtained through the acquisition of high resolution parametric images.

Blood oxygen level-dependent MRI (BOLD-MRI)

Method used in functional MRI to observe variations in oxygen concentration within tissues based on the oxy-deoxyhaemoglobin ratio.

Relaxation rate ($R2^*$)

Rate of signal decay in MRI using a $T2^*$ -weighted gradient-echo sequence, and is the inverse of the time constant $T2^*$. $R2^*$ is sensitive to tissue oxygenation levels and the presence of iron oxide particles.

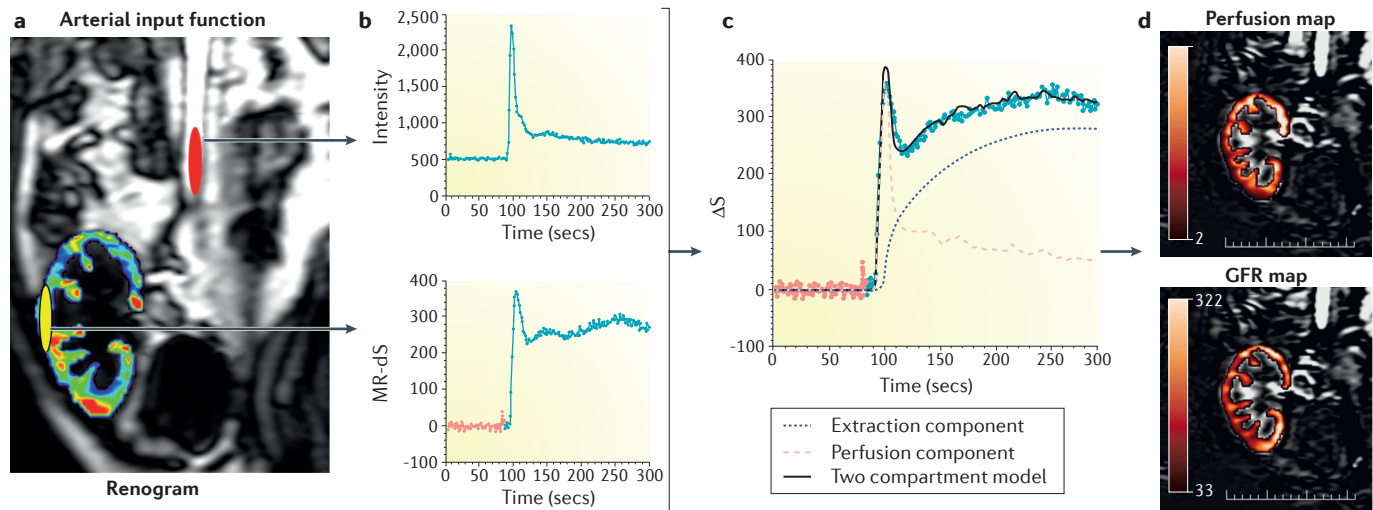


Figure 5 | Principles of quantitative dynamic contrast-enhanced (DCE)-MRI applied to a kidney transplant. DCE-MRI measures the transit of a tracer to estimate various parameters, such as perfusion or glomerular filtration rate. **a** | The renogram is a map of the maximal signal intensity that can be obtained after injection of a gadolinium-based tracer bolus. **b** | By placing a region of interest on the aorta (red) and on the cortex (yellow), signal intensity time curves (kinetic curves) can be produced. The aortic kinetic curve enables characterization of the shape of the bolus (arterial input function). **c** | A two-compartment model is applied to these kinetic data to extract the perfusion component and the extraction component. **d** | Quantitative maps of perfusion and glomerular filtration rate (GFR; in ml/min/g of tissue) can be generated from these data, respectively.

cortical $T2^*$ -value in normal kidneys (FIG. 6). Although $T2^*$ has a linear correlation with intrarenal pO_2 values ($r=0.67-0.73$)⁷⁸ and can, therefore, be considered a surrogate marker of tissue oxygenation, variations in $T2^*$ can be associated with changes in oxygen consumption, blood flow, and blood volume, which makes physiopathologic interpretation of these $T2^*$ changes somewhat difficult.

Dynamic changes in oxygenation can be induced by various stimuli, such as pharmacologic agents or hydration status. In young individuals, hydration inhibits active reabsorption in the medullary tubules and increases medullary flow, thus resulting in an increase in oxygenation (represented as an increase in medullary $T2^*$). This response to hydration is usually reduced in the elderly⁷⁹. Medullary oxygenation in animal models was reduced by inhibition of prostaglandins and nitric oxide, and by intravenous injection of radiocontrast agents⁷⁹. In a rat model of diabetic nephropathy, the shortest $T2^*$ was found within the outer stripe of the outer medulla, which indicates the presence of hypoxia due either to hyperfiltration or changes in renal blood volume³³.

The first renal application of comparative dynamic BOLD-MRI in humans was performed in patients with diabetic mellitus with no microalbuminuria, hypertension, or renal insufficiency. These patients failed to present any marked improvement in medullary oxygenation after water loading; thus the data obtained by BOLD-MRI provided an early biomarker of renal involvement in diabetes^{80,81}. An analysis of 37 patients with CKD found that the decrease in $T2^*$ cortical values (indicating hypoxia) correlated with the percentage of fibrotic area on renal biopsy; the degree of hypoxia increased with the

extent of fibrosis ($R^2=0.23$)⁸². Conversely, no association was identified between $T2^*$ and eGFR or CKD stage in a large cohort of patients with CKD⁸³.

In atherosclerotic renal artery stenosis a decrease in $T2^*$ was reported in normal sized kidneys, downstream of high-grade stenosis, which increased after administration of furosemide, but no prognostic value could be established⁸⁴. Hypoxia is mediated by activation of the angiotensin type 1 receptor by angiotensin II⁸⁵. Renin-angiotensin blockade can improve cortical and medullary oxygenation by inhibiting the production of angiotensin II, as shown in hypertensive patients with atherosclerotic renal artery stenosis^{86,87}, and in patients with diabetic or non-diabetic CKD⁸⁸. Medullary pO_2 is reportedly higher in renal allografts, (as indicated by a higher $T2^*$ value following BOLD-MRI) compared to native kidneys of healthy volunteers^{2,89}, which might be explained by reduced oxygen consumption secondary to reduced active reabsorption of sodium. In the context of acute allograft rejection, most studies have shown higher medullary oxygenation in the failing graft compared to normally functioning grafts or grafts with acute tubular necrosis. This effect is likely due to impairment of renal tubular function (including oxygen consumption) as a result of leukocyte infiltration^{90,91}.

Even though BOLD-MRI seems to be a very exciting, yet challenging, technique that can provide insights into our understanding of CKD pathophysiology, some discrepancies have started to emerge, mainly in the data produced from analyses of native kidneys⁹². Technical challenges in the utility of BOLD-MRI remain, as signal intensity is influenced by various factors including hydration status, sodium avidity, vascular volume, and

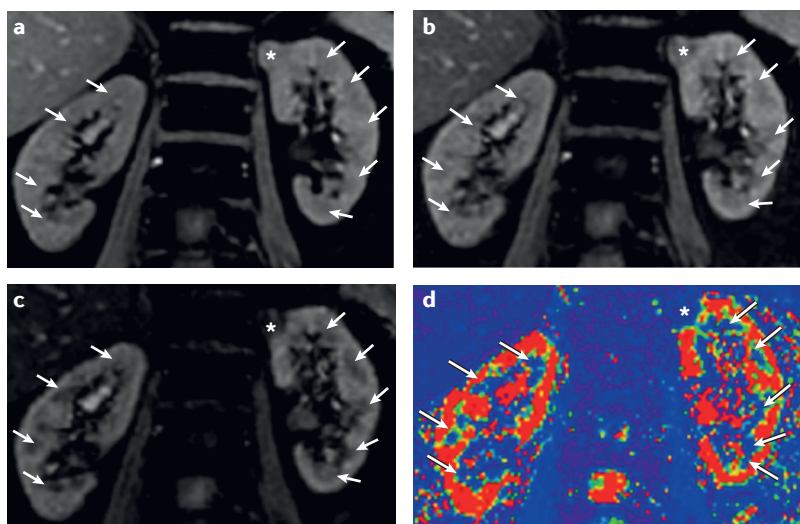


Figure 6 | Intrarenal blood oxygen level-dependent MRI in a patient with a small tumour in the upper pole of the left kidney. a–c | The applied $T2^*$ -weighted MRI sequence is characterized by an increased sensitivity to the level of paramagnetic deoxyhemoglobin by increasing the echo-time. A progressive decrease in signal intensity is detected within the medulla (arrows) and within the tumour (asterisks) due to a lower level of tissue partial pressure of oxygen (PO_2). **d** | A parametric image of the relaxation time $T2^*$ (or of the relaxation rate $R2^* = 1/T2^*$) can be generated by fitting signal intensity versus echo-time data to an exponential function on a voxel by voxel basis. Lower $T2^*$ values (blue) are observed within the medulla (arrows) and within the tumour (asterisk) indicative of lower tissue PO_2 , compared to the cortex (red), which has a higher $T2^*$ and, therefore, a higher PO_2 .

vessel geometry as well as other factors that affect oxygen dissociation. Furthermore, although BOLD-MRI might be able to detect differences in tissue oxygen levels, it cannot be used to differentiate between the various underlying causative factors⁹². New approaches for the quantification of changes in signal intensity — namely the determination of fractional tissue hypoxia (the percentage of the entire axial section with an $R2^*$ value $>30/\text{sec}$) — have been proposed to increase the reliability and reproducibility of this technique^{93,94}. Moreover, a better understanding of the observed signal changes is still necessary by implementation of an experimental integrated setup that combines simultaneous measurement of $R2^*$ and tissue perfusion in each renal compartment^{93,94}.

Vascular resistance. Doppler ultrasonography can also be used to identify intrarenal haemodynamic changes that are suggestive of functional and/or structural deterioration. The Doppler-derived renal resistive index is a sonographic index that quantifies the complex changes in vascular resistance, compliance, and cross-sectional areas associated with the intricate flow and tissue changes that can occur in conditions such as arteriosclerosis and interstitial fibrosis⁹⁵. This index is sensitive to systemic haemodynamics, such as systemic pulse pressure and heart rate.

The potential to use the renal resistive index as a predictive parameter in a variety of vascular and renal diseases has gained interest, despite the low specificity of this approach. In a meta-analysis, Ninet *et al.*⁹⁶

showed that the resistive index might predict persistent AKI in critically ill patients by distinguishing transient from persistent AKI; however, many factors can influence the resistive index, and so the utility of a single resistive index measurement at intensive care admission to determine optimal mean arterial pressure remains uncertain⁹⁷. In patients with diabetic and non-diabetic CKD, a resistive index value >0.8 is associated with a fast decline in renal function over 5 years⁹⁸. In atherosclerotic renal artery stenosis, a resistive index in the contralateral kidney >0.73 was found to be an independent predictor of renal function failure after revascularization⁹⁹. In the setting of primary hypertension, the resistive index is now considered an accurate independent predictor of poor cardiovascular and renal outcomes¹⁰⁰.

The utility of the renal resistive index to assess the function of renal allografts is complex because the value of resistive index could depend on characteristics of both the organ donor and the recipient. This complexity might explain some of the discrepancies observed in the literature. For example, an increase in the resistive index in the early post-transplantation period was shown to correlate with long-term transplant function ($P < 0.001$)¹⁰¹, but another study that measured the resistive index at several time points found that the value reflected recipient characteristics, such as age at transplantation or age at death, but not the functional characteristics of the graft¹⁰². This field is in need of further investigation and experience.

Renal ultrafiltration

Split renal function. Measurement of split (or differential) renal function is widely used by urologists to guide the management of unilateral uropathies (mainly obstruction and tumours). In the field of nephrology, measurement of split renal function might be required when reduced renal function is associated with renal asymmetry (as in renovascular diseases) to calculate a single kidney GFR when coupled with a global clearance value. In routine clinical practice, split renal function is still measured by renal scintigraphy, which requires the use of glomerular (^{99m}Tc -DTPA) or tubular (^{99m}Tc -MAG3) radiotracers. Many medical practitioners have promoted a move away from nuclear medicine techniques and the use of radioactive material towards radiology. Numerous single-centre studies have reported correlations between differential CT morphologic criteria, such as renal parenchymal area⁵¹, parenchymal volume¹⁰³ or a combination of volume and attenuation¹⁰⁴, but validation on a large scale has not yet been performed.

Split renal function can be obtained using radiologic functional approaches, such as DCE-CT or DCE-MRI, by applying the same algorithms used for renal scintigraphy. A large, multicentre trial compared renal scintigraphy with DCE-MRI in a cohort of adults and children with unilateral obstruction (see [Supplementary information S5](#) (figure)). Good reproducibility for both methods, and equivalent results were obtained in patients with moderately dilated

Scintigraphy

2D imaging of the distribution of radioactivity after administration of a radio-pharmaceutical imaging agent with affinity for the organ of interest. Scintigraphy enables evaluation of kidney function.

kidneys, with a difference of $1.2 \pm 12\%$ between the techniques, making substitution acceptable. However, in severely dilated kidneys, DCE–MRI underestimated the mean split function by $4 \pm 13\%$, making substitution questionable¹⁰⁵.

Regional glomerular filtration rate. An estimation of the GFR is the best index to monitor CKD, and reference methods, such as radionuclide clearances, are underutilized as they are relatively time consuming and require several blood and/or urinary samples. GFR is thus estimated in clinical practice based on creatinine and/or cystatin C serum concentrations, despite several pitfalls, which are outside the scope of this Review. Fast, quantitative methods based on intrarenal tracer kinetics, such as DCE–CT and DCE–MRI, which do not require blood and/or urine sampling could be extremely useful for clinical patient management. As for perfusion studies, dynamic image acquisition is performed after injection of an iodine contrast agent or low molecular weight gadolinium chelates that are pure glomerular tracers. The duration of image acquisition is extended to the entire filtration phase and a two-compartment or a three-compartment pharmacokinetic model is applied to extract GFR values for each kidney^{70,73}. Functional maps of GFR can be obtained, making it possible to measure regional filtration rates.

DCE–CT was shown to have moderate agreement with iothalamate-derived single kidney GFR (standard error of the estimate of $14.0 \text{ ml/min/1.73 m}^2$ using an extended gamma-variate model)¹⁰⁶, but this method required injection of a high-dose iodine contrast agent (0.5 ml/kg) at an elevated rate of 10 ml/s through a central catheter positioned in the right atrium. DCE–MRI, which is used to measure perfusion, can also be used to estimate GFR with a low dose of intravenous gadolinium chelate (FIG. 5). Lim *et al.*¹⁰⁷ obtained good agreement in GFR values obtained from DCE–MRI and radioisotopic technique, with a mean difference of $-0.7 \text{ ml/min/1.73 m}^2$ (95% CI -12 – 11). In another study, the median difference between the DCE–MRI and radioisotopes ranged between -4.1 and $-7.7 \text{ ml/min/1.73 m}^2$ (REF. 108). Even with encouraging reports from single-centre studies in native^{109,110} and transplanted kidneys¹¹¹, no clear consensus can be discerned regarding the optimal choice of technique¹¹², the sequence parameters for MRI, or the type of mathematical model to assess GFR.

Other functional parameters

Renal metabolism. Magnetic resonance spectroscopy (MRS) can detect nuclei such as carbon (^{13}C), nitrogen (^{15}N), fluorine (^{19}F), sodium (^{23}Na), phosphorus (^{31}P) and hydrogen (^1H), and has been used to identify biochemical changes associated with disease in a variety of organs, including the kidneys¹¹³. The low sensitivity of MRS, however, has limited the development of this technique. Methods based on injection of hyperpolarized ^{13}C -labelled molecules (such as ^{13}C -pyruvate) markedly enhances ^{13}C detection and has allowed for metabolic imaging of several substrates *in vivo*, including fumarate and pyruvate¹¹⁴. MRS of hyperpolarized $[1,4\text{-}^{13}\text{C}]$

fumarate allowed the detection of early tubular necrosis and its distinction from glomerular inflammation in murine models¹¹⁵.

Intrarenal sodium concentration. The distribution of intrarenal sodium is characterized by a cortico–medullary gradient, is essential for the urinary concentrating process, and has a close association with renal function. Maril *et al.*^{116,117} were the first to demonstrate and quantify the intrarenal sodium gradient by MRI, which requires specifically tuned coils to detect the magnetic resonance signal. Changes in signal intensity in excised kidneys were directly proportional to tissue sodium concentration, and both administration of furosemide or urinary obstruction could elicit marked and distinct alterations to the medullary sodium profiles; these results were confirmed in 2011 in a series of 28 volunteers¹¹⁸. In rat kidneys with acute tubular necrosis, the sodium gradient between the cortex and outer medulla and between the cortex and inner medulla was reduced by 21% and 40%, respectively, compared to control kidneys¹¹⁹. Further experience in the utility of this technique to monitor the intrarenal sodium gradient is required to define the value of such data and its clinical impact.

Intrarenal pH. Tissue pH is generally measured using proton MRS. MRI is also able to measure pH *in vivo* using pH-sensitive gadolinium complexes, such as gadolinium-DOTA-4AmP5 (REF. 120). These techniques, however, remain underutilized because of the low sensitivity and limited availability of gadolinium complexes. A new approach of signal amplification with saturation exchange (known as chemical exchange saturation transfer) demonstrated the ability of an iodinated contrast agent, iopamidol, to measure pH values and induced pH alterations in healthy mice¹²¹.

Conclusions

The techniques outlined in this Review have the potential to provide new biomarkers of renal disease that can be useful for patient management and to predict clinical and functional renal outcomes. Radiologic imaging is moving from solely generating a depiction of organ anatomy and macroscopic tissue changes towards providing a measurement of quantitative, functional, and structural parameters. The field of nephrology is expected to benefit from this movement as renal tissue changes predominantly occur at the microscopic level, often require a biopsy for diagnosis, and are associated with numerous contributors to functional disturbance. At present, only nuclear medicine techniques can accurately report parameters of renal function, such as perfusion or GFR, and these techniques remain a reference for the evaluations made in clinical practice. Ultrasonography — which already provides haemodynamic biomarkers of tissue changes, such as resistive index — will probably extend its contribution to the understanding of structural changes associated with renal diseases upon incorporation of elastography techniques. In the near future, we expect that MRI will also become a major imaging technique for the evaluation of renal parenchymal disease, based on

Magnetic resonance spectroscopy (MRS)

A complement to MRI that uses information derived from different atoms to determine the concentration of metabolites in the tissue examined.

its flexibility and ability to provide anatomic, structural, and functional information. Many magnetic resonance parameters can be obtained without the administration of a contrast agent, which is an important issue due to the multiple restrictions of their use in the context of renal function impairment.

Despite these advances, more experience is required to better understand the pathophysiological mechanisms that drive some of the macroscopic and microscopic

changes that can be detected by these new radiologic techniques. Centres of excellence will need to propose steps to harmonize the technical requirements of the different imaging systems, and then large-scale evaluation of the variability and validity of these techniques, as well as their clinical impact, will be mandatory. We hope that many of these techniques will be implemented in clinical practice in the near future to improve the management and diagnosis of renal diseases.

- Zhang, J. L., Rusinek, H., Chandarana, H. & Lee, V. S. Functional MRI of the kidneys. *J. Magn. Reson. Imaging* **37**, 282–293 (2013).
- Thoeny, H. C. & De Keyser, F. Diffusion-weighted MR imaging of native and transplanted kidneys. *Radiology* **259**, 25–38 (2011).
- Khawaja, A. Z. *et al.* Revisiting the risks of MRI with Gadolinium based contrast agents — review of literature and guidelines. *Insights Imaging* **6**, 553–558 (2015).
- McDonald, J. S. *et al.* Risk of intravenous contrast material-mediated acute kidney injury: a propensity score-matched study stratified by baseline-estimated glomerular filtration rate. *Radiology* **271**, 65–73 (2014).
- Widjaja, E. *et al.* Ultrasound measured renal length versus low dose CT volume in predicting single kidney glomerular filtration rate. *Br. J. Radiol.* **77**, 759–764 (2004).
- van den Dool, S. W., Wasser, M. N., de Fijter, J. W., Hoekstra, J. & van der Geest, R. J. Functional renal volume: quantitative analysis at gadolinium-enhanced MR angiography — feasibility study in healthy potential kidney donors. *Radiology* **236**, 189–195 (2005).
- Coulam, C. H., Bouley, D. M. & Sommer, F. G. Measurement of renal volumes with contrast-enhanced MRI. *J. Magn. Reson. Imaging* **15**, 174–179 (2002).
- Rigalleau, V. *et al.* Large kidneys predict poor renal outcome in subjects with diabetes and chronic kidney disease. *BMC Nephrol.* **11**, 3 (2010).
- Vivier, P.-H. *et al.* *In vitro* assessment of a 3D segmentation algorithm based on the belief functions theory in calculating renal volumes by MRI. *AJR Am. J. Roentgenol.* **191**, W127–W134 (2008).
- Cheung, C. M. *et al.* MR-derived renal morphology and renal function in patients with atherosclerotic renovascular disease. *Kidney Int.* **69**, 715–722 (2006).
- Semelka, R. C. *et al.* Renal corticomedullary differentiation: observation in patients with differing serum creatinine levels. *Radiology* **190**, 149–152 (1994).
- Chung, J. J., Semelka, R. C. & Martin, D. R. Acute renal failure: common occurrence of preservation of corticomedullary differentiation on MR images. *Magn. Reson. Imaging* **19**, 789–795 (2001).
- Faubel, S., Patel, N. U., Lockhart, M. E. & Cadnapaphornchai, M. A. Renal relevant radiology: use of ultrasonography in patients with AKI. *Clin. J. Am. Soc. Nephrol.* **9**, 382–394 (2014).
- Jeong, J. Y., Kim, S. H., Lee, H. J. & Sim, J. S. Atypical low-signal-intensity renal parenchyma: causes and patterns. *Radiographics* **22**, 833–846 (2002).
- Chapman, A. B. *et al.* Renal structure in early autosomal-dominant polycystic kidney disease (ADPKD): the Consortium for Radiologic Imaging Studies of Polycystic Kidney Disease (CRISP) cohort. *Kidney Int.* **64**, 1035–1045 (2003).
- Bae, K. T. *et al.* MRI-based kidney volume measurements in ADPKD: reliability and effect of gadolinium enhancement. *Clin. J. Am. Soc. Nephrol.* **4**, 719–725 (2009).
- Grantham, J. J. *et al.* Volume progression in polycystic kidney disease. *N. Engl. J. Med.* **354**, 2122–2130 (2006).
- Torres, V. E. *et al.* Tolvaptan in patients with autosomal dominant polycystic kidney disease. *N. Engl. J. Med.* **367**, 2407–2418 (2012).
- Kurschat, C. E. *et al.* An approach to cystic kidney diseases: the clinician's view. *Nat. Rev. Nephrol.* **10**, 687–699 (2014).
- Corot, C., Robert, P., Idée, J. M. & Port, M. Recent advances in iron oxide nanocrystal technology for medical imaging. *Adv. Drug Deliv. Rev.* **1**, 1471–1504 (2006).
- Hauger, O. *et al.* Nephrotoxic nephritis and obstructive nephropathy: evaluation with MR imaging enhanced with ultrasmall superparamagnetic iron oxide-preliminary findings in a rat model. *Radiology* **217**, 819–826 (2000).
- Ye, Q. *et al.* *In vivo* detection of acute rat renal allograft rejection by MRI with USPIO particles. *Kidney Int.* **61**, 1124–1135 (2002).
- Jo, S.-K. *et al.* Detection of inflammation following renal ischemia by magnetic resonance imaging. *Kidney Int.* **64**, 43–51 (2003).
- Beckmann, N. *et al.* Macrophage infiltration detected at MR imaging in rat kidney allografts: early marker of chronic rejection? *Radiology* **240**, 717–724 (2006).
- Hauger, O. *et al.* USPIO-enhanced MR imaging of macrophage infiltration in native and transplanted kidneys: initial results in humans. *Eur. Radiol.* **17**, 2898–2907 (2007).
- Hedgire, S. S. *et al.* Evaluation of renal quantitative T2* changes on MRI following administration of ferumoxytol as a T2* contrast agent. *Int. J. Nanomedicine* **9**, 2101–2107 (2014).
- Chae, E. Y. *et al.* Allogeneic renal graft rejection in a rat model: *in vivo* MR imaging of the homing trait of macrophages. *Radiology* **256**, 847–854 (2010).
- Sargsyan, S. A. *et al.* Detection of glomerular complement C3 fragments by magnetic resonance imaging in murine lupus nephritis. *Kidney Int.* **81**, 152–159 (2012).
- Serkova, N. J. *et al.* Renal inflammation: targeted iron oxide nanoparticles for molecular MR imaging in mice. *Radiology* **255**, 517–526 (2010).
- Grabner, A. *et al.* Noninvasive imaging of acute renal allograft rejection by ultrasound detection of microbubbles targeted to T-lymphocytes in rats. *Ultraschall Med.* **37**, 82–91 (2016).
- Moghazi, S. *et al.* Correlation of renal histopathology with sonographic findings. *Kidney Int.* **67**, 1515–1520 (2005).
- Lee, V. S. *et al.* Is increased echogenicity related to a decrease in glomerular filtration rate? Objective measurements in pediatric solitary kidney patients — a retrospective analysis. *PLoS ONE* **10**, e0133577 (2015).
- Ries, M. *et al.* Renal diffusion and BOLD MRI in experimental diabetic nephropathy. *J. Magn. Reson. Imaging* **17**, 104–113 (2003).
- Thoeny, H. C., De Keyser, F., Oyen, R. H. & Peeters, R. R. Diffusion-weighted MR imaging of kidneys in healthy volunteers and patients with parenchymal diseases: initial experience. *Radiology* **235**, 911–917 (2005).
- Xu, Y., Wang, X. & Jiang, X. Relationship between the renal apparent diffusion coefficient and glomerular filtration rate: preliminary experience. *J. Magn. Reson. Imaging* **26**, 678–681 (2007).
- Togao, O. *et al.* Assessment of renal fibrosis with diffusion-weighted MR imaging: study with murine model of unilateral ureteral obstruction. *Radiology* **255**, 772–780 (2010).
- Ries, M., Jones, R. A., Basseau, F., Moonen, C. T. & Grenier, N. Diffusion tensor MRI of the human kidney. *J. Magn. Reson. Imaging* **14**, 42–49 (2001).
- Grenier, N., Gennissin, J.-L., Cornelis, F., Le Bras, Y. & Couzi, L. Ultrasound elastography of the kidney. *Ultrasound Clin.* **8**, 551–564 (2013).
- Paparo, F. *et al.* Real-time elastography in the assessment of liver fibrosis: a review of qualitative and semi-quantitative methods for elastogram analysis. *Ultrasound Med. Biol.* **40**, 1923–1933 (2014).
- Gao, J. *et al.* Renal transplant elasticity ultrasound imaging: correlation between normalized strain and renal cortical fibrosis. *Ultrasound Med. Biol.* **39**, 1536–1542 (2013).
- Orlacchio, A. *et al.* Kidney transplant: usefulness of real-time elastography (RTE) in the diagnosis of graft interstitial fibrosis. *Ultrasound Med. Biol.* **40**, 2564–2572 (2014).
- Gennissin, J.-L., Grenier, N., Combe, C. & Tanter, M. Supersonic shear wave elastography of *in vivo* pig kidney: influence of blood pressure, urinary pressure and tissue anisotropy. *Ultrasound Med. Biol.* **38**, 1559–1567 (2012).
- Grenier, N., Gennissin, J. L., Cornelis, F., Le Bras, Y. & Couzi, L. Renal ultrasound elastography. *Diagn. Interv. Imaging* **94**, 545–550 (2013).
- Syversveen, T. *et al.* Tissue elasticity estimated by acoustic radiation force impulse quantification depends on the applied transducer force: an experimental study in kidney transplant patients. *Eur. Radiol.* **22**, 2130–2137 (2012).
- Asano, K. *et al.* Acoustic radiation force impulse elastography of the kidneys: is shear wave velocity affected by tissue fibrosis or renal blood flow? *J. Ultrasound Med.* **33**, 793–801 (2014).
- Guo, L.-H. *et al.* Acoustic radiation force impulse imaging for noninvasive evaluation of renal parenchyma elasticity: preliminary findings. *PLoS ONE* **8**, e68925–e68928 (2013).
- Yu, N., Zhang, Y. & Xu, Y. Value of virtual touch tissue quantification in stages of diabetic kidney disease. *J. Ultrasound Med.* **33**, 787–792 (2014).
- Goya, C. *et al.* Acoustic radiation force impulse imaging for evaluation of renal parenchyma elasticity in diabetic nephropathy. *AJR Am. J. Roentgenol.* **204**, 324–329 (2015).
- Grenier, N. *et al.* Quantitative elastography of renal transplants using supersonic shear imaging: a pilot study. *Eur. Radiol.* **22**, 2138–2146 (2012).
- Lee, C. U. *et al.* MR elastography in renal transplant patients and correlation with renal allograft biopsy: a feasibility study. *Acad. Radiol.* **19**, 834–841 (2012).
- Feder, M. T., Blitstein, J., Mason, B. & Hoenig, D. M. Predicting differential renal function using computerized tomography measurements of renal parenchymal area. *J. Urol.* **180**, 2110–2115 (2008).
- Kline, T. L. *et al.* Utilizing magnetization transfer imaging to investigate tissue remodeling in a murine model of autosomal dominant polycystic kidney disease. *Magn. Reson. Med.* **75**, 1466–1473 (2015).
- Caravan, P. *et al.* Collagen-targeted MRI contrast agent for molecular imaging of fibrosis. *Angew. Chem. Int. Ed. Engl.* **46**, 8171–8173 (2007).
- Bull, S. *et al.* Human non-contrast T1 values and correlation with histology in diffuse fibrosis. *Heart* **99**, 932–937 (2013).
- Hueper, K. *et al.* T1-mapping for assessment of ischemia-induced acute kidney injury and prediction of chronic kidney disease in mice. *Eur. Radiol.* **24**, 2252–2260 (2014).
- Wang, F. *et al.* Longitudinal assessment of mouse renal injury using high-resolution anatomic and magnetization transfer MR imaging. *Magn. Reson. Imaging* **32**, 1125–1132 (2014).
- Ito, K. *et al.* Magnetization transfer MR imaging of the kidney: evaluation at 3.0T in association with renal function. *Eur. Radiol.* **23**, 2315–2319 (2013).
- Peng, X.-G. *et al.* Renal lipids and oxygenation in diabetic mice: noninvasive quantification with MR imaging. *Radiology* **269**, 748–757 (2013).
- Tögel, F. E. & Westenfelder, C. Kidney protection and regeneration following acute injury: progress through stem cell therapy. *Am. J. Kidney Dis.* **60**, 1012–1022 (2012).
- Bussolati, B. & Camussi, G. Therapeutic use of human renal progenitor cells for kidney regeneration. *Nat. Rev. Nephrol.* **11**, 695–706 (2015).

61. Bos, C. *et al.* *In vivo* MR imaging of intravascularly injected magnetically labeled mesenchymal stem cells in rat kidney and liver. *Radiology* **233**, 781–789 (2004).
62. Ilttrich, H. *et al.* *In vivo* magnetic resonance imaging of iron oxide-labeled, arterially-injected mesenchymal stem cells in kidneys of rats with acute ischemic kidney injury: detection and monitoring at 3T. *J. Magn. Reson. Imaging* **25**, 1179–1191 (2007).
63. Hauger, O. *et al.* MR evaluation of the glomerular homing of magnetically labeled mesenchymal stem cells in a rat model of nephropathy. *Radiology* **238**, 200–210 (2006).
64. Torres, V. E. *et al.* Magnetic resonance measurements of renal blood flow and disease progression in autosomal dominant polycystic kidney disease. *Clin. J. Am. Soc. Nephrol.* **2**, 112–120 (2007).
65. Schoenberg, S. O. *et al.* Morphologic and functional magnetic resonance imaging of renal artery stenosis: a multireader tricenter study. *J. Am. Soc. Nephrol.* **13**, 158–169 (2002).
66. Gillis, K. A. *et al.* Inter-study reproducibility of arterial spin labelling magnetic resonance imaging for measurement of renal perfusion in healthy volunteers at 3 Tesla. *BMC Nephrol.* **15**, 23 (2014).
67. Wang, L. *et al.* Diagnostic value of quantitative contrast-enhanced ultrasound (CEUS) for early detection of renal hyperperfusion in diabetic kidney disease. *J. Nephrol.* **28**, 669–678 (2015).
68. Piscaglia, F. *et al.* The EFSUMB guidelines and recommendations on the clinical practice of contrast enhanced ultrasound (CEUS): update 2011 on non-hepatic applications. *Ultraschall Med.* **33**, 33–59 (2012).
69. Lemoine, S. *et al.* Renal perfusion: noninvasive measurement with multidetector CT versus fluorescent microspheres in a pig model. *Radiology* **260**, 414–420 (2011).
70. Bokacheva, L., Rusinek, H., Zhang, J. L. & Lee, V. S. Assessment of renal function with dynamic contrast-enhanced MR imaging. *Magn. Reson. Imaging Clin. N. Am.* **16**, 597–611 (2008).
71. Attenberger, U. I., Morelli, J. N., Schoenberg, S. O. & Michaely, H. J. Assessment of the kidneys: magnetic resonance angiography, perfusion and diffusion. *J. Cardiovasc. Magn. Reson.* **13**, 70 (2011).
72. Sourbron, S. Compartmental modelling for magnetic resonance renography. *Z. Med. Phys.* **20**, 101–114 (2010).
73. Bokacheva, L., Rusinek, H., Zhang, J. L., Chen, Q. & Lee, V. S. Estimates of glomerular filtration rate from MR renography and tracer kinetic models. *J. Magn. Reson. Imaging* **29**, 371–382 (2009).
74. Haase, V. H. Mechanisms of hypoxia responses in renal tissue. *J. Am. Soc. Nephrol.* **24**, 537–541 (2013).
75. Miyata, T. & van Ypersele de Strihou, C. Diabetic nephropathy: a disorder of oxygen metabolism? *Nat. Rev. Nephrol.* **6**, 83–95 (2009).
76. Takiyama, Y. & Haneda, M. Hypoxia in diabetic kidneys. *Biomed. Res. Int.* **2014**, 837421 (2014).
77. Brezis, M. & Rosen, S. Hypoxia of the renal medulla — its implications for disease. *N. Engl. J. Med.* **9**, 647–655 (1995).
78. Pedersen, M. *et al.* Validation of quantitative BOLD MRI measurements in kidney: application to unilateral ureteral obstruction. *Kidney Int.* **67**, 2305–2312 (2005).
79. Prasad, P. V., Priatna, A., Spokes, K. & Epstein, F. H. Changes in intrarenal oxygenation as evaluated by BOLD MRI in a rat kidney model for radiocontrast nephropathy. *J. Magn. Reson. Imaging* **13**, 744–747 (2001).
80. Epstein, F. H., Veves, A. & Prasad, P. V. Effect of diabetes on renal medullary oxygenation during water diuresis. *Diabetes Care* **25**, 575–578 (2002).
81. Economides, P. A. *et al.* Kidney oxygenation during water diuresis and endothelial function in patients with type 2 diabetes and subjects at risk to develop diabetes. *Metabolism* **53**, 222–227 (2004).
82. Inoue, T. *et al.* Noninvasive evaluation of kidney hypoxia and fibrosis using magnetic resonance imaging. *J. Am. Soc. Nephrol.* **22**, 1429–1434 (2011).
83. Michaely, H. J. *et al.* Renal BOLD-MRI does not reflect renal function in chronic kidney disease. *Kidney Int.* **81**, 684–689 (2012).
84. Textor, S. C. *et al.* The use of magnetic resonance to evaluate tissue oxygenation in renal artery stenosis. *J. Am. Soc. Nephrol.* **19**, 780–788 (2008).
85. Welch, W. J., Baumgärtl, H., Lübbers, D. & Wilcox, C. S. Renal oxygenation defects in the spontaneously hypertensive rat: role of AT1 receptors. *Kidney Int.* **63**, 202–208 (2003).
86. Siddiqi, L. *et al.* Inhibition of the renin-angiotensin system affects kidney tissue oxygenation evaluated by magnetic resonance imaging in patients with chronic kidney disease. *J. Clin. Hypertens. (Greenwich)* **16**, 214–218 (2014).
87. Gloviczki, M. L. *et al.* Preserved oxygenation despite reduced blood flow in poststenotic kidneys in human atherosclerotic renal artery stenosis. *Hypertension* **55**, 961–966 (2010).
88. Manotham, K. *et al.* Angiotensin II receptor blocker partially ameliorated intrarenal hypoxia in chronic kidney disease patients: a pre-/post-study. *Int. Med. J.* **42**, e33–e37 (2012).
89. Thoeny, H. C. *et al.* Functional evaluation of transplanted kidneys with diffusion-weighted and BOLD MR imaging: initial experience. *Radiology* **241**, 812–821 (2006).
90. Sadowski, E. A. *et al.* Blood oxygen level-dependent and perfusion magnetic resonance imaging: detecting differences in oxygen bioavailability and blood flow in transplanted kidneys. *Magn. Reson. Imaging* **28**, 56–64 (2010).
91. Han, F. *et al.* The significance of BOLD MRI in differentiation between renal transplant rejection and acute tubular necrosis. *Nephrol. Dial. Transplant.* **23**, 2666–2672 (2008).
92. Neugarten, J. & Golestaneh, L. Blood oxygenation level-dependent MRI for assessment of renal oxygenation. *Int. J. Nephrol. Renovasc. Dis.* **7**, 421–435 (2014).
93. Saad, A. *et al.* Human renovascular disease: estimating fractional tissue hypoxia to analyze blood oxygen level-dependent MR. *Radiology* **268**, 770–778 (2013).
94. Pohlmann, A. *et al.* Detailing the relation between renal T2* and renal tissue pO2 using an integrated approach of parametric magnetic resonance imaging and invasive physiological measurements. *Invest. Radiol.* **49**, 547–560 (2014).
95. Bude, R. O. & Rubin, J. M. Effect of downstream cross-sectional area of an arterial bed on the resistive index and the early systolic acceleration. *Radiology* **212**, 732–738 (1999).
96. Ninet, S. *et al.* Doppler-based renal resistive index for prediction of renal dysfunction reversibility: a systematic review and meta-analysis. *J. Crit. Care* **30**, 629–635 (2015).
97. Dewitte, A. *et al.* Doppler resistive index to reflect regulation of renal vascular tone during sepsis and acute kidney injury. *Crit. Care* **16**, R165 (2012).
98. Radermacher, J., Ellis, S. & Haller, H. Renal resistance index and progression of renal disease. *Hypertension* **39**, 699–703 (2002).
99. Bruno, R. M. *et al.* Predictive role of renal resistive index for clinical outcome after revascularization in hypertensive patients with atherosclerotic renal artery stenosis: a monocentric observational study. *Cardiovasc. Ultrasound* **12**, 9 (2014).
100. Doi, Y. *et al.* Renal resistive index and cardiovascular and renal outcomes in essential hypertension. *Hypertension* **60**, 770–777 (2012).
101. McArthur, C., Geddes, C. C. & Baxter, G. M. Early measurement of pulsatility and resistive indexes: correlation with long-term renal transplant function. *Radiology* **259**, 278–285 (2011).
102. Naesens, M. *et al.* Intrarenal resistive index after renal transplantation. *N. Engl. J. Med.* **369**, 1797–1806 (2013).
103. Herts, B. R. *et al.* Estimating glomerular filtration rate in kidney donors: a model constructed with renal volume measurements from donor CT scans. *Radiology* **252**, 109–116 (2009).
104. Summerlin, A. L. *et al.* Determination of split renal function by 3D reconstruction of CT angiograms: a comparison with gamma camera renography. *AJR Am. J. Roentgenol.* **191**, 1552–1558 (2008).
105. Claudon, M. *et al.* Chronic urinary obstruction: evaluation of dynamic contrast-enhanced MR urography for measurement of split renal function. *Radiology* **273**, 801–812 (2014).
106. Kwon, S. H., Saad, A., Herrmann, S. M., Textor, S. C. & Lerman, L. O. Determination of single-kidney glomerular filtration rate in human subjects by using CT. *Radiology* **276**, 490–498 (2015).
107. Lim, S. W., Chrysochou, C., Buckley, D. L., Kalra, P. A. & Sourbron, S. P. Prediction and assessment of responses to renal artery revascularization with dynamic contrast-enhanced magnetic resonance imaging: a pilot study. *Am. J. Physiol. Renal Physiol.* **305**, F672–F678 (2013).
108. Vivier, P.-H. *et al.* Kidney function: glomerular filtration rate measurement with MR renography in patients with cirrhosis. *Radiology* **259**, 462–470 (2011).
109. Hackstein, N., Kooijman, H., Tomaselli, S. & Rau, W. S. Glomerular filtration rate measured using the Patlak plot technique and contrast-enhanced dynamic MRI with different amounts of gadolinium-DTPA. *J. Magn. Reson. Imaging* **22**, 406–414 (2005).
110. Lee, V. S. *et al.* Renal function measurements from MR renography and a simplified multicompartmental model. *Am. J. Physiol. Renal Physiol.* **292**, F1548–F1559 (2007).
111. Yamamoto, A. *et al.* Quantitative evaluation of acute renal transplant dysfunction with low-dose three-dimensional MR renography. *Radiology* **260**, 781–789 (2011).
112. Grenier, N. *et al.* Measurement of glomerular filtration rate with magnetic resonance imaging: principles, limitations, and expectations. *Semin. Nucl. Med.* **38**, 47–55 (2008).
113. Tugnoli, V. & Tosi, M. R. Biochemical characterization of human brain and kidney tissues by magnetic resonance spectroscopy. *Ital. J. Biochem.* **52**, 80–86 (2003).
114. Gallagher, F. A. *et al.* Production of hyperpolarized [1,4-¹³C]malate from [1,4-¹³C]fumarate is a marker of cell necrosis and treatment response in tumors. *Proc. Natl. Acad. Sci. USA* **106**, 19801–19806 (2009).
115. Clatworthy, M. R. *et al.* Magnetic resonance imaging with hyperpolarized [1,4-¹³C]fumarate allows detection of early renal acute tubular necrosis. *Proc. Natl. Acad. Sci. USA* **109**, 13374–13379 (2012).
116. Maril, N. *et al.* Sodium MRI of the human kidney at 3 Tesla. *Magn. Reson. Med.* **56**, 1229–1234 (2006).
117. Maril, N., Margalit, R., Mispelner, J. & Degani, H. Functional sodium magnetic resonance imaging of the intact rat kidney. *Kidney Int.* **65**, 927–935 (2004).
118. Haneder, S. *et al.* Quantitative and qualitative ²³Na MR imaging of the human kidneys at 3T: before and after a water load. *Radiology* **260**, 857–865 (2011).
119. Maril, N., Margalit, R., Rosen, S., Heyman, S. N. & Degani, H. Detection of evolving acute tubular necrosis with renal ²³Na MRI: studies in rats. *Kidney Int.* **69**, 765–768 (2006).
120. Raghunand, N., Howison, C., Sherry, A. D., Zhang, S. & Gillies, R. J. Renal and systemic pH imaging by contrast-enhanced MRI. *Magn. Reson. Med.* **49**, 249–257 (2003).
121. Longo, D. L., Busato, A., Lanzardo, S., Antico, F. & Aime, S. Imaging the pH evolution of an acute kidney injury model by means of iopamidol, a MRI-CEST pH-responsive contrast agent. *Magn. Reson. Med.* **70**, 859–864 (2012).

Acknowledgements

This work was achieved within the context of the Laboratory of Excellence TRAIL ANR-10-LABX-57. The authors would like to thank Pippa McKelvie-Sebileau, University of Bordeaux, France, for her editorial assistance prior to submission.

Author contributions

N.G. and C.C. researched the data and wrote the article. N.G., C.C. P.M. made substantial contributions to discussion of the content and reviewed and/or edited the manuscript before submission.

Competing interests statement

N.G. is a member of the advisory board of Supersonic Imagine, Aix-en-Provence, France. P.M. and C.C. declare no competing interests.

SUPPLEMENTARY INFORMATION

See online article: [S1](#) (figure) | [S2](#) (figure) | [S3](#) (figure) | [S4](#) (figure) | [S5](#) (figure)

ALL LINKS ARE ACTIVE IN THE ONLINE PDF